All-Electrical Determination of Crystal Orientation in Anisotropic Two-Dimensional Materials

Lintao Peng, Spencer A. Wells, Christopher R. Ryder, Mark C. Hersam, and Matthew Grayson

Phys. Rev. Lett. **120**, 086801 — Published 21 February 2018

DOI: 10.1103/PhysRevLett.120.086801

All-electrical determination of crystal orientation in anisotropic two-dimensional materials

Lintao Peng[1+], Spencer A. Wells[2+], Christopher R. Ryder[2], Mark C. Hersam[1,2,3,4`*], and Matthew Grayson[1,3*]

[1]Applied Physics Graduate Program, Northwestern University, Evanston, IL 60208, USA

[2]Department of Materials Science and Engineering, Northwestern University, Evanston, IL 60208, USA

[3]Department of Electrical Engineering and Computer Science, Northwestern University, Evanston, IL 60208, USA

[4]Department of Chemistry, Northwestern University, Evanston, IL 60208, USA

[+]These authors contributed equally to this work

*Corresponding authors: m-grayson@northwestern.edu; m-hersam@northwestern.edu

Abstract: The crystal orientation of an exfoliated black phosphorous (BP) flake is determined by purely electrical means. A sequence of three resistance measurements on an arbitrarily shaped flake with five contacts determines the three independent components of the anisotropic in-plane resistivity tensor, thereby revealing the crystal axes. The resistivity anisotropy ratio decreases linearly with increasing temperature T and carrier-density reaching a maximum ratio of 3.0 at low temperatures and densities, while mobility indicates impurity scattering at low T and acoustic phonon scattering at high T.

Layered two-dimensional (2D) materials, also called van der Waals materials, have anisotropic crystal structure, allowing micromechanical exfoliation into thin sheets. However, many important 2D materials including black phosphorus (BP), GaTe, ReS_2, SnS and WTe_2 possess additional in-plane structural anisotropy that manifests as an anisotropic in-plane resistance[1-5]. For example, BP is a high mobility layered semiconductor with bandgap from 0.3 eV to 1.7 eV as its thickness is decreased from bulk to monolayer[1,6-8]. Its properties have been demonstrated in electronics as field-effect transistors[1,2,9] and optoelectronics as photodetectors[10,11]. Of particular importance are the anisotropic properties of BP, including quasi-1D excitons in the monolayer limit; a half-linear, half-parabolic dispersion under hydrostatic pressure; and anisotropic negative Poisson's ratio under compression.[12-16] All such anisotropic studies require identification of the crystallographic orientation of BP, which until now has required polarized Raman and optical reflection spectroscopy.[2,7,11,17] However, there currently exists no electrical method to accurately measure the crystal orientation in as-exfoliated BP. Prior electrical methods to quantify anisotropy have strict geometric constraints on the sample shape and/or crystallographic orientation, limiting their utility with exfoliated materials.[18-21] The radial starburst contact pattern commonly employed in 2D anisotropy characterization is only qualitatively accurate due to the two-point series contact resistances and the short-circuiting of current through the many peripheral contacts.[2,22]

Here, an all-electrical technique quantifies the anisotropic resistivity tensor of arbitrarily shaped few-layer flakes of BP, thereby revealing in-plane crystal orientation. Three or more four-point resistance measurements that use at least five contacts at the periphery of a thin flake can determine the three unknowns – the *c*- and *a*-axis resistivity, and anisotropy angle – via geometric transformations including conformal mapping. The crystallographic orientation

deduced from this all-electrical conformal five-contact (C5C) method is confirmed with polarized Raman spectroscopy. For the first time, both temperature and carrier density dependence of the electrical anisotropy are reported in the same flake in an exfoliated 2D material.

Devices were fabricated using black phosphorus micromechanically exfoliated onto a degenerately doped Si wafer with a 300 nm thermal SiO_2 film. This served as the gate electrode and gate dielectric respectively. Electron beam lithography was used to define device features, and the electrodes consisted of thermally evaporated Ni/Au 10/40 nm. In order to minimize oxidation during processing, the device was stored in a glovebox, and anhydrous 1-methyl-2-pyrrolidone was used for resist liftoff. After device fabrication, alumina was deposited *via* atomic layer deposition in order to encapsulate the device.

There are a total of three unknowns in the 2D anisotropy problem. Here we parameterize them as the anisotropy angle θ between the *x*-*y* lab basis and the *c*-*a* crystal basis, the sheet resistivity determinant ${\rho_s}^2 = \|\boldsymbol{\rho}\|$, and a geometric anisotropy scaling factor $\alpha = \sqrt[4]{\rho_{cc}/\rho_{aa}} \leq 1$. The *c*-*a* axes represent the right-handed coordinate system for the armchair and zig-zag directions in black phosphorus, respectively, and θ subtends the angle between the laboratory *x*-axis and the crystal *c*-axis. Though in general no analytical expression can solve these three unknowns in terms of measured four-point resistances, it is nonetheless straightforward to compute the inverse problem, namely to calculate the four-point resistance value R_k for a given sample shape and contact configuration k when the parameters ρ_s, θ, and α are known. From such an expression, each four-point resistance measurement then constrains the space of possible

ρ_s, θ, and α values, and the intersection of three such subspaces from three different measurements will define the unique solution for ρ_s, θ, and α.

The first step is therefore to calculate this 4-point resistance function R_k for the sample shape of interest in terms of prescribed ρ_s, θ, and α parameters. A photograph of the exfoliated flake will be used to define a polygon approximation to the sample shape, and three coordinate transformations will be performed that each preserve the resistivity determinant. As an example, consider the polygon-shaped sample in Fig. 1a with $V = 7$ geometric vertices. The anisotropic 2D resistivity direction set by θ is depicted graphically with rectangular cross-hatched lines, where the widely (closely) spaced green (blue) lines represent the high- (low-) resistivity direction. Of these seven vertices, $N = 5$ represent contacts, labeled A-E. The contacts can also be located along flat edges using the same coordinate transformations and analysis. Because each transformation preserves the resistivity determinant, the sheet resistivity scale ρ_s can be factored out of the expression for the four-point resistance:

$$R_k(\rho_s, \theta, \alpha) = \rho_s \cdot f_k(\theta, \alpha). \qquad (1)$$

The resulting geometric function $f_k(\theta, \alpha)$ for a given sample geometry and contact configuration k depends on the rotation and scale transformation variables θ and α, respectively. The first transformation (Fig. 1b) is a counter-clockwise rotation by the anisotropy angle θ from the *x*-*y* lab basis to the *c*-*a* crystal basis. The second transformation (Fig. 1c) is an anisotropic scaling[23] where the new *c'*-*a'* axes are scaled by $1/\alpha$ and α, respectively, and the anisotropy scaling factor α maps the original *anisotropic* conductor to an equivalent *isotropic* conductor with the same sheet resistivity determinant:

$$\begin{pmatrix} c' \\ a' \end{pmatrix} = \begin{pmatrix} 1/\alpha & 0 \\ 0 & \alpha \end{pmatrix} \begin{pmatrix} \cos\theta & \sin\theta \\ -\sin\theta & \cos\theta \end{pmatrix} \begin{pmatrix} x \\ y \end{pmatrix} \qquad (2)$$

The third and final determinant-preserving step is the reverse Schwarz-Christoffel transformation. A *forward* Schwarz-Christoffel transformation [24] maps a coordinate $w = u + iv$ in the upper half *u*-*v* plane to a point $\zeta = c' + ia'$ within a polygon in the *c'*-*a'* plane according the complex integral,

$$\zeta(w) = \int_0^w \frac{1}{(\zeta-u_1)^{1-\beta_1/\pi}(\zeta-u_2)^{1-\beta_2/\pi}(\zeta-u_3)^{1-\beta_3/\pi}\ldots} d\zeta \quad (3)$$

where the u_i are points along the *u*-axis in the *u*-*v* plane which map to vertices (c'_i, a'_i) of the polygon in the *c'*-*a'* plane with subtended vertex angles β_i. The *reverse* Schwarz-Christoffel transformation is simply the computational inverse of this one-to-one mapping, from the polygon to the upper half-plane[25]. The geometric function for any four-point resistance can now be calculated analytically from the point u_i along the boundary of the semi-infinite plane[26]:

$$f_{lm,np} = \frac{1}{\pi}\ln\left[\frac{(u_n-u_l)(u_p-u_m)}{(u_p-u_l)(u_n-u_m)}\right] \equiv f_k. \qquad (4)$$

Here *l, m* label the $\pm$ current and *n, p* the $\pm$ voltage contact pairs, respectively, of the k^{th} contact configuration, where $k = \{1, ..., M\}$ for the total number of $M = 2\binom{N}{4}$ independent configurations.

In practice, the number Q of four-point resistances actually measured is typically more than three, and the unknowns ρ_s, θ, and α are determined from a simple variance minimization based on Eq. (1). Solving Eq. (1) to define a parametric dependence of the sheet resistivity on the transformation parameters $\rho_{s,k}(\theta,\alpha) = R_k/f_k(\theta,\alpha)$, the normalized variance σ of the candidate sheet resistivities can be written as a function of θ and α

$$\sigma(\theta,\alpha) = \frac{1}{\langle \rho_{s,k}(\theta,\alpha)\rangle}\sqrt{\frac{\sum_{k=1}^{Q}\left[\rho_{s,k}(\theta,\alpha)-\langle \rho_{s,k}(\theta,\alpha)\rangle\right]^2}{Q}}. \quad (5)$$

The coordinates (θ_0, α_0) that minimize this variance reveal the unique solution for the crystallographic orientation θ_0 and anisotropy scaling factor α_0. The sheet resistance is then the average value at the point of minimum variance $\rho_{s,0} = \langle \rho_{s,k}(\theta_0, \alpha_0)\rangle$. The final 2D anisotropic resistivity tensor becomes $\rho_{cc} = \alpha_0^2\, \rho_{s,0}$ and $\rho_{aa} = \alpha_0^{-2}\, \rho_{s,0}$.

The variance minimization C5C method was applied to sample A (Fig. 1d, inset), whose polygon approximation was introduced above. Sample A is a d = 31 nm thick micromechanically exfoliated BP flake with sheet carrier density p = 1.77×10^{12} cm^{-2} measured at 300 K. The resulting variance $\sigma(\theta, \alpha)$ of Q = 10 different measured contact configurations is shown in Fig. 1e. Because the variance $\sigma(\theta, \alpha) = \sigma(\theta + 180°, \alpha)$ is periodic with period 180°, the minimum can be uniquely represented in a 2θ polar plot whereby the graphical angle is twice the anisotropy angle θ, and the isotropic condition $\alpha = 1$ is at the polar center. The global minimum is observed at $\theta_0 = 93°$ and $\alpha_0 = 0.85$ yielding $\rho_{s,0} = 11 \pm 1$ kΩ with anisotropy ratio $r = \frac{\rho_{aa}}{\rho_{cc}} = \alpha_0^{-4} = 1.9$. This result is consistent with previous reported values on both bulk[27] and thin flake BP devices[2,28].

Because sheet resistance in *isotropic* 2D samples is often measured with the van der Pauw (vdP) technique, we introduce a second, equivalent C5C method for measuring *anisotropic* resistivity, which we call the vdP parametric intersection method (Figure 1f). Consider two four-point resistances R_k and $R_{k'}$ chosen such that k and k' are vdP pairs of measurement contacts, whereby the same four contacts are used such as ABCD, but cyclically permuted among the

current and voltage contacts, such as k = {AB, DC} and k' = {BC, AD}.[26] From the two resistance measurements R_k and $R_{k'}$, the standard vdP method gives the value for the isotropic sheet resistivity ρ_s, which for anisotropic samples represents the square-root-determinant resistivity[23] and sets a parametric constraint on $\alpha(\theta)$. For example, figure 1f shows $M = Q/2 = 5$ different parametric curves $\alpha(\theta)$ on a 2θ polar plot for the five possible sets of four contacts. Wherever any two curves intersect, a consistent solution of α and θ exists, and the final solution is the average of (ρ_s, θ, α) at all intersections. For sample A, the result is $\rho_{s,0} = 11 \pm 1$ kΩ, $\theta_0 = 93° \pm 3°$, and $\alpha_0 = 0.85 \pm 0.01$, such that $r = 1.9 \pm 0.1$ in excellent agreement with the C5C variance-minimization results. To confirm the conformal five-contact methods in Fig. 2, we investigated an MoS_2 device sample C with thickness d = 8 nm that is *not* expected to show anisotropy. The result confirms a very weak anisotropy of only $\alpha_0 = 0.99$ and $r = \alpha_0^{-4} = 1.05$, with the variance minimum in the center of the radial plot, with degenerate solutions of θ_0 and a sheet resistivity $\rho_{s,0} = 69$ kΩ.

The anisotropy angle θ_0 determined by the C5C method in BP sample A (Fig. 3a) was independently verified using polarized Raman spectroscopy (Fig. 3b). Polarizing the incident 532 nm laser parallel to the detector polarization, the armchair (c-axis) and zigzag (a-axis) directions of BP can be determined.[17] Raman measurements of the BP flake were taken by rotating the material in 10-degree increments, generating polarization-dependent Raman spectra. By fitting intensities of the A_g^2 spectra,[29] the angle of minimum Raman intensity is $\theta_R = 97° \pm 5°$ (Fig. 3c), in agreement with the more accurate C5C measurement of $\theta_0 = 93° \pm 3°$ (Fig. 3a). Note that the encapsulation of the BP flake with atomic layer deposited alumina protects against

accelerated degradation due to laser irradiation, and that the laser wavelength was chosen to be transparent to the alumina.[30]

The utility of this method is illustrated by studying temperature- and hole density-dependence on another BP sample (sample B) with thickness d = 28 nm that has N = 6 contacts. Here Q = 14 contact combination measurements were chosen, since more measurements allow greater redundancy in 4-point resistance measurements and greater accuracy in anisotropy calibration. From these measurements, the anisotropy angle is θ_0 = 68° at 300 K, agreeing again with Raman spectroscopy (results not shown) within $\pm$5°, and the anisotropy ratio is r = 2.5, for sheet carrier density $p = 4.78\times10^{11}$ cm^{-2}.

The temperature dependence of the anisotropy ratio was studied by holding the hole density of sample B fixed at $p = 2.0\times10^{12}$ cm^{-2} with gate bias. As shown in Fig. 4a, both a- and c-direction mobilities show positive power-law increase in the low-temperature range up to 180 K, saturating at high-temperature. This behavior is consistent with strong impurity scattering at low temperatures and the onset of acoustic phonon scattering at high-temperatures, as reported in BP[2,31] and other 2D materials[32,33]. These measurements reveal that the anisotropy ratio r increases linearly as T is decreased, while the anisotropy angle θ_0 remains constant (Fig. 4d). The observed temperature trend of the anisotropy ratio matches the prediction for remote-ionized-impurity scattering(Ref. 35). Interestingly, Fig. 4b shows that the linearly decreasing trend continues even as the experiment crosses over to the high-temperature phonon-limited regime that theoretical studies have yet to investigate.

Examining the gate-voltage dependence in sample B, the mobility along the a- and c-directions is measured as a function of sheet carrier density from $p = 5.3\times10^{11}$ to 4.4×10^{12} cm^{-2}, whereby mobilities in both directions increase with increasing carrier density (Fig. 4c) consistent

with theoretical prediction[34,35]. The anisotropy ratio itself decreases slightly as density increases, while the angle of anisotropy θ_0 remains constant (Fig. 4d). This observed decrease in anisotropy is consistent with theory for this charged impurity-dominated regime, and the weak dependence indicates that a prevailing number of the impurities are within or close to the BP layer itself.[34,35]

In conclusion, the conformal five-contact (C5C) method employs a conformal mapping method to enable all-electrical determination of the in-plane crystallographic orientation and full resistivity tensor in arbitrarily shaped anisotropic 2D materials. Testing exfoliated BP and MoS_2, both variance minimization and vdP parametric intersection methods are shown to yield consistent results. The utility of the C5C method is demonstrated with temperature and carrier density dependence of the anisotropy in exfoliated BP. Since the C5C technique can be universally applied without the strict geometric restrictions of other electrical techniques or the material-specific knowledge required for optical spectra interpretation, it can advance fundamental studies and accelerate device development in the rapidly growing field of anisotropic 2D materials.

Acknowledgments

This research was supported by the Air Force Office of Scientific Research (FA9550-15-1-0247) and the National Science Foundation Materials Research Science and Engineering Center (MRSEC) of Northwestern University (DMR-1121262).

References

[1] H. Liu, A. T. Neal, Z. Zhu, Z. Luo, X. Xu, D. Tomanek, and P. D. Ye, ACS Nano. **8**, 4033 (2014).
[2] F. Xia, H. Wang, and Y. Jia, Nat. Commun. **5**, 4458 (2014).
[3] S. Huang *et al.*, ACS Nano. **10**, 8964 (2016).
[4] D. A. Chenet, O. B. Aslan, P. Y. Huang, C. Fan, A. M. van der Zande, T. F. Heinz, and J. C. Hone, Nano. Lett. **15**, 5667 (2015).
[5] Z. Tian, C. Guo, M. Zhao, R. Li, and J. Xue, ACS Nano **11**, 2219 (2017).
[6] V. Tran, R. Soklaski, Y. Liang, and L. Yang, Phys. Rev. B **89**, 235319 (2014).
[7] J. Qiao, X. Kong, Z. X. Hu, F. Yang, and W. Ji, Nat. Commun. **5**, 4475 (2014).
[8] L. Li *et al.*, Nat. Nanotech. **12**, 21 (2017).
[9] L. Li, Y. Yu, G. J. Ye, Q. Ge, X. Ou, H. Wu, D. Feng, X. H. Chen, and Y. Zhang, Nat. Nanotech. **9**, 372 (2014).
[10] M. Buscema, D. J. Groenendijk, S. I. Blanter, G. A. Steele, H. S. van der Zant, and A. Castellanos-Gomez, Nano. Lett. **14**, 3347 (2014).
[11] H. Yuan, *et al.*, Nat. Nanotech. **10**, 707 (2015).
[12] X. Wang, *et al.*, Nat. Nanotech. **10**, 517 (2015).
[13] R. Fei, T. Vy, and Y. Li. Phys. Rev. B **91**, 195319 (2015).
[14] Z. J. Xiang, *et al.*, Phys. Rev. Lett. **115**, 186403 (2015).
[15] Y. Du, J. Maassen, W. Wu, Z. Luo, X. Xu, and P. D. Ye, Nano. Lett. **16**, 6701 (2016).
[16] X. Liu, C. R. Ryder, S. A. Wells, and M. C. Hersam, Small Methods **1**, 1700143 (2017).
[17] X. Ling *et al.*, Nano. Lett. **16**, 2260 (2016).
[18] O. Bierwagen, R. Pomraenke, S. Eilers, and W. T. Masselink, Phys. Rev. B **70**, 165307 (2004).
[19] S. Asmontas, V. Kleiza and J. Kleiza, ACTA Phys. Pol. A **113**, 1559 (2008).
[20] C. A. M. dos Santos, A. de Campos, M. S. da Luz, B. D. White, J. J. Neumeier, B. S. de Lima, and C. Y. Shigue, J. Appl. Phys. **110**, 083703 (2011).
[21] K. A. Borup, K. F. F. Fischer, D. R. Brown, G. J. Snyder, and B. B. Iversen, Phys. Rev. B **92,** 045210 (2015).
[22] G. Qiu *et al.*, Nano. Lett. **16**, 7364 (2016).
[23] v. d. Pauw, Philips Res. Repts **16**, 187 (1961).
[24] P. A. A. L. Roland Schinzinger, Conformal Mapping Methods and Applications (2003).
[25] T. A. Driscoll, Schwarz-Christoffel toolbox，http://www.math.udel.edu/~driscoll/SC/.
[26] v. d. Pauw, Philips Res. Repts **13**, 9 (1958).
[27] S. E. Yuichi Akahama, Shin-ichiro Narita, J. Phys. Soc. Jpn. **52**, 2148 (1983).
[28] A. Mishchenko, Y. Cao, G. L. Yu, C. R. Woods, R. V. Gorbachev, K. S. Novoselov, A. K. Geim, and L. S. Levitov, Nano. Lett. **15**, 6991 (2015).
[29] T. Low, A. S. Rodin, A. Carvalho, Y. Jiang, H. Wang, F. Xia, and A. H. Castro Neto, Phys. Rev. B **90**, 075434 (2014).
[30] J. D. Wood, *et al.*, Nano Lett. **12**, 6964 (2014)
[31] N. Gillgren *et al.*, 2D Materials **2**, 011001 (2014).
[32] J. H. Chen, C. Jang, S. Adam, M. S. Fuhrer, E. D. Williams, and M. Ishigami, Nat. Phys. **4**, 377 (2008).
[33] B. Radisavljevic and A. Kis, Nat. Mater. **12**, 815 (2013).

[34] Y. Liu, T. Low, and P. P. Ruden, Phys. Rev. B **93**, 165402 (2016).
[35] Y. Liu and P. P. Ruden, Phys. Rev. B **95**, 165446 (2017).

Figures

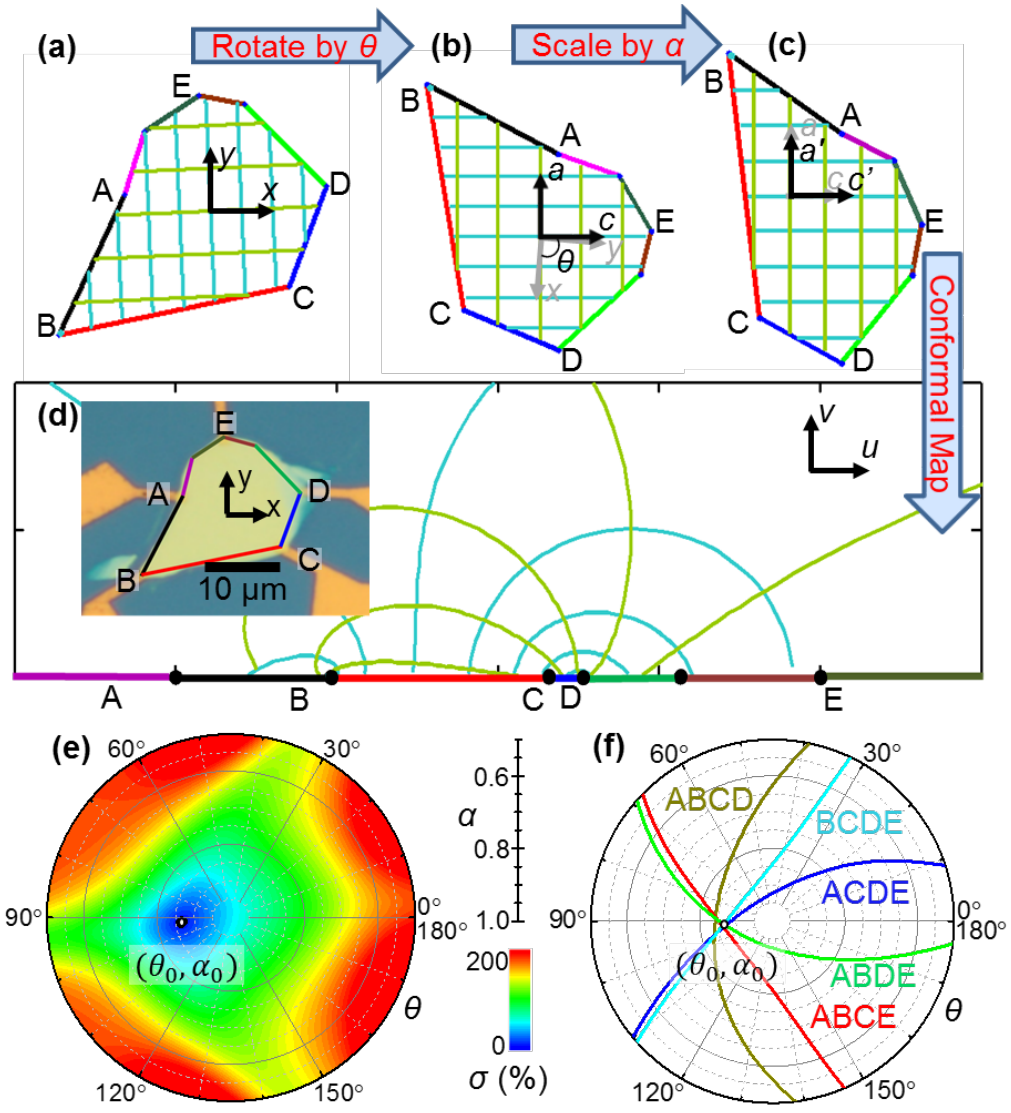

Figure 1. Conformal five-contact method on *anisotropic* BP sample A. (a) Polygon approximation of sample in *x*-*y* lab frame; (b) Rotation by θ to the *c*-*a* crystal axes; (c) Anisotropic scaling of crystal axes by $1/\alpha$ and α, respectively, to equivalent *isotropic* resistivity sample in *c'*-*a'* basis; (d) Conformal mapping to semi-infinite *u*-*v* plane. Inset photo: sample A in lab frame overlaid with polygon approximation. All four-point resistances of original anisotropic sample are identical to those of semi-infinite plane. (e) Color plot of normalized variance $\sigma(\alpha, \theta)$ from Eq. (3) on a 2θ polar plot: minimum variance at θ_0 = 93° and α_0 = 0.85 (r = 1.9), where $\rho_{s,0} = 11$ kΩ. (f) Parametric intersection method for various $\alpha(\theta)$ curves on a 2θ polar plot. Variance minimization method results in (e) agree with parametric intersection results in (f).

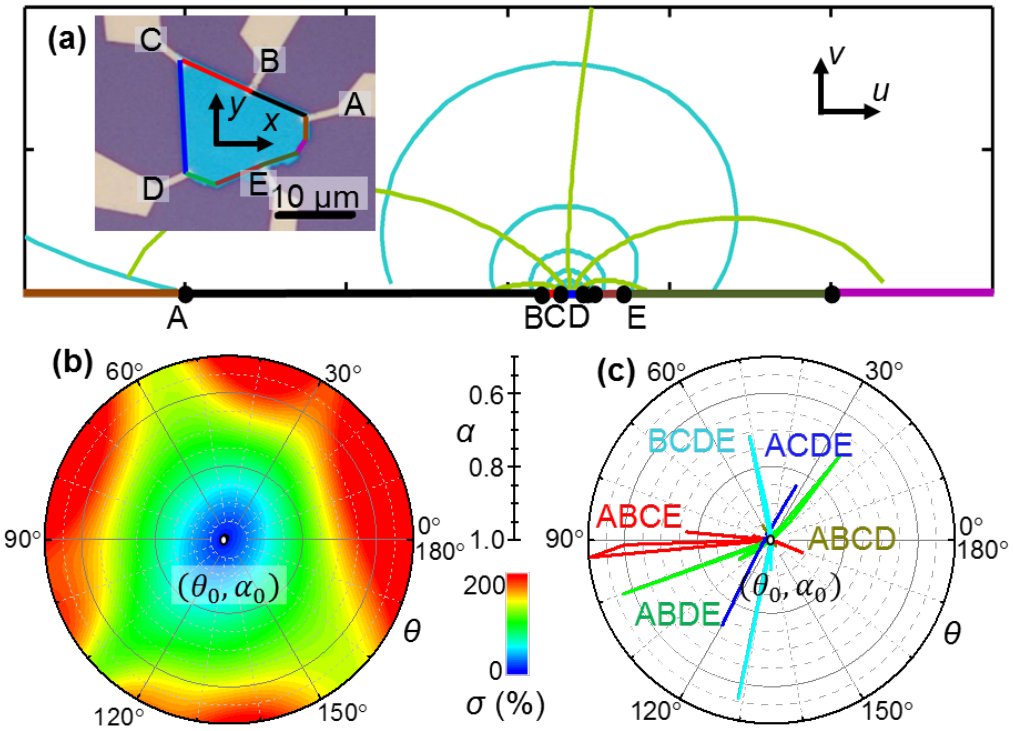

Figure 2. Conformal five-contact method on *isotropic* MoS_2 sample C. (a) Inset photo: sample C in lab frame overlaid with polygon approximation; main panel shows conformal mapping to semi-infinite *u*-*v* plane. (b) Color plot of normalized variance $\sigma(\alpha, \theta)$ (Eq. 3) on a 2θ polar plot: minimum variance at $\alpha_0 = 0.99$ ($r = 1.05$) at center of polar plot, where $\rho_{s,0} = 69\ \text{k}\Omega$. (c) Parametric intersection method for various $\alpha(\theta)$ curves on a 2θ polar plot. Variance minimization results in (b) agree with parametric intersection results in (c).

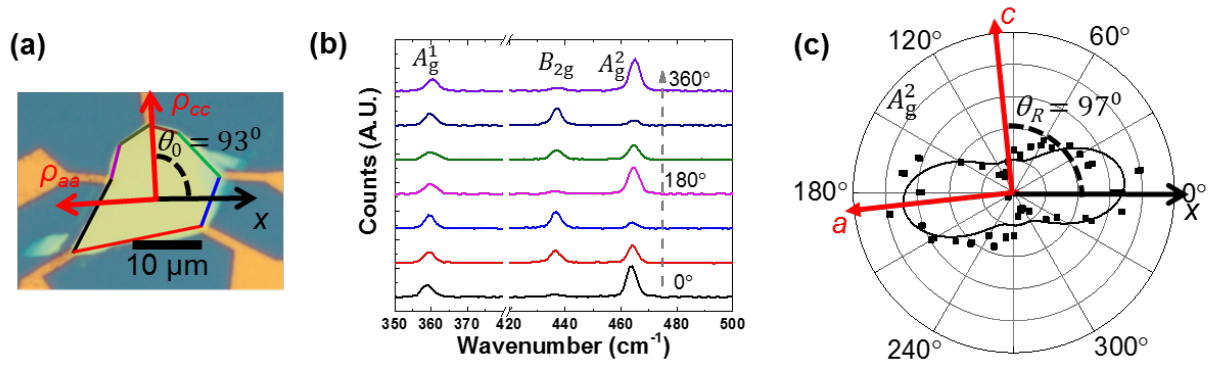

Figure 3. Comparison between anisotropy angle determined by C5C method and polarized Raman spectrum on BP sample A. (a) Crystal orientation determined by C5C method in Fig. 1 is $\theta_0 = 93° \pm 3°$; (b) Selected polarized Raman spectra on sample A with polarization angle rotating from 0° to 360°; (c) Radiii of black dots on the polar plot represent peak amplitudes for polarized Raman intensities of the A_g^2 peak, with the black curve representing a theoretical fit. Resulting Raman crystal orientation angle is $\theta_R = 97° \pm 5°$ in agreement with more accurate θ_0 from C5C method.

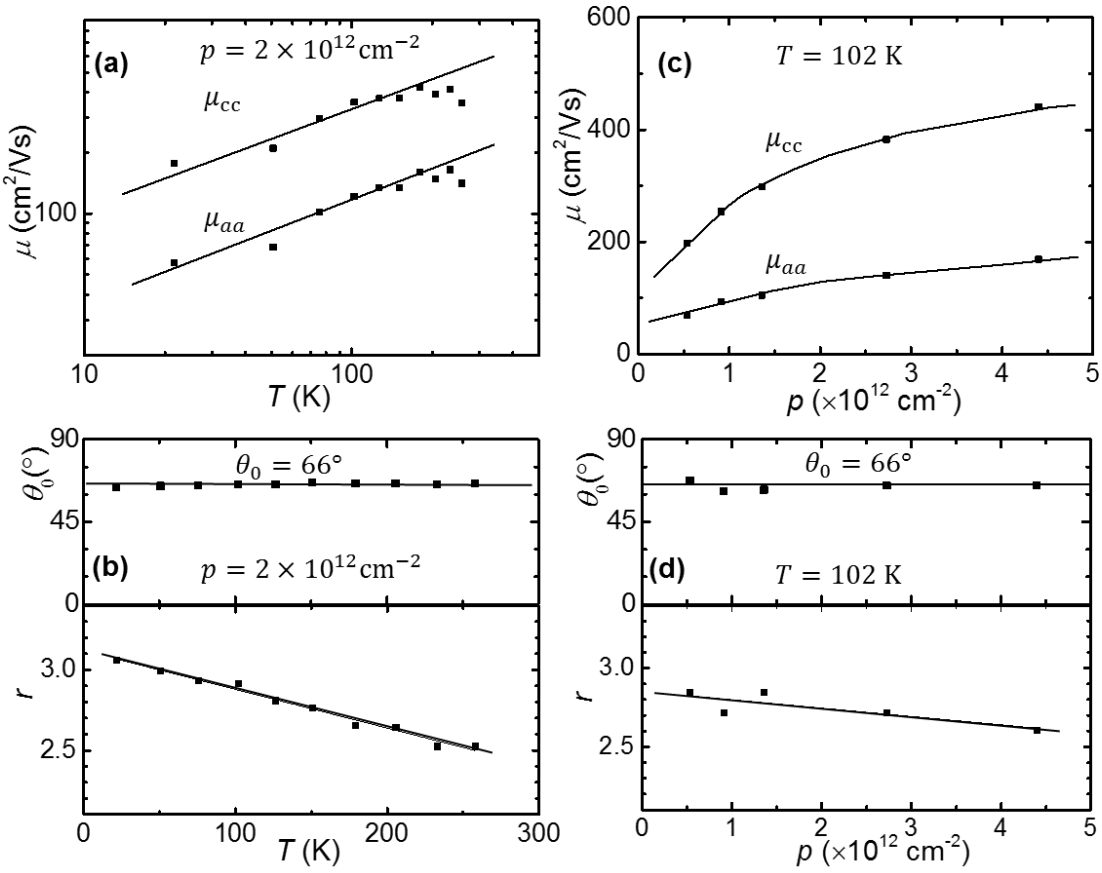

Figure 4. Anisotropy analysis on BP sample B (d = 28 nm) as function of density and temperature. Curves are guides to the eye. (a) Temperature dependence: at fixed density, carrier mobilities μ_{cc} and μ_{aa} along the armchair and zig-zag directions, respectively, both increase with a power-law in the low-temperature range, before saturating at high-temperatures, indicating the onset of phonon scattering; (b) At fixed density, anisotropy angle θ_0 (top panel) remains constant and ratio r (bottom panel) decreases linearly with temperature. (c) Density dependence: Carrier mobilities μ_{cc} and μ_{aa} increase with increasing carrier density. (d) Anisotropy angle θ_0 (top panel) remains constant while the anisotropy ratio r (bottom panel) decreases slightly with carrier density.